ACS OMEGA

Open Access

http://pubs.acs.org/journal/acsodf

Article

Surface Plasmon Resonance Modulation by Complexation of Platinum on the Surface of Silver Nanocubes

Avi Huri, Yaakov Mandelbaum, Mike Rozenberg, Anya Muzikansky, Melina Zysler, and David Zitoun*

Cite This: *ACS Omega* 2024, 9, 35526−35536

Read Online

ACCESS | Metrics & More | Article Recommendations | Supporting Information

ABSTRACT: The use of plasmonic particles, specifically, localized surface plasmonic resonance (LSPR), may lead to a significant improvement in the electrical, electrochemical, and optical properties of materials. Chemical modification of the dielectric constant near the plasmonic surface should lead to a shift of the optical resonance and, therefore, the basis for color tuning and sensing. In this research, we investigated the variation of the LSPR by modifying the chemical environment of Ag nanoparticles (NPs) through the complexation of Pt(IV) metal cations near the plasmonic surface. This study is carried out by measuring the shift of the plasmon dipole resonance of Ag nanocubes (NCs) and nanowires (NWs) of differing sizes upon coating the Ag surface with a layer of polydopamine (PDA) as a coordinating matrix for Pt(IV) complexes. The red shift of up to 45 nm depends linearly on the thickness of the PDA/Pt(IV) layer and the Pt(IV) content. Additionally, we calculated the dielectric constant of the surrounding medium using a numerical method.

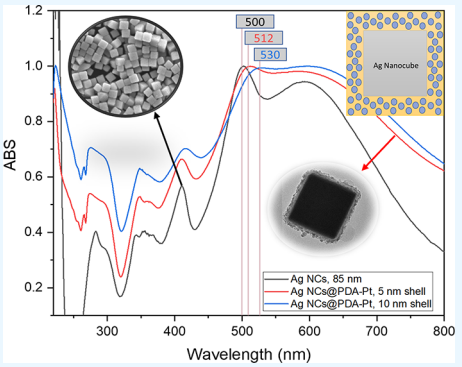

1. INTRODUCTION

Plasmonic nanoparticles (NPs) are promising materials with unique optical properties. The strong interaction of their surface with rays of light on a nanometer scale causes the conversion of light energy in electron gas oscillation, named plasmon, on their surface. As a result, plasmonic NPs are able to function as nanoantennas and scatter or concentrate the light in an effective way[1] (which can be predicted by the Mie theory for spherical NPs).[2] Therefore, plasmons have found a wide number of applications in physical and biological sensors,[3−9] photovoltaic cells,[10,11] photocatalysis,[10,12,13] surface-enhanced Raman spectroscopy (SERS),[6,9,14] and more.[15]

There are two types of plasmonic resonance. Both of these can be induced via irradiation by light and result in oscillation at the same frequency as the exciting wavelength: surface plasmon resonance (SPR) and localized surface plasmon resonance (LSPR). SPR refers to vibrations propagating along a planar surface, and LSPR refers to the local resonance confined within NPs. The coherent electronic oscillation occurs at the interface between the metal NPs and a dielectric medium.

Since the plasmon phenomenon depends on the spatial fluctuations of the electrons and their density on the surface, the composition, size, and shape of the particle have a great influence. In addition, the dielectric medium around the particle is of great importance.[6,16,17]

Most plasmonic particles are noble metals, especially silver and gold. The great advantage of a noble metal is its high chemical stability and relative biological compatibility. However, the plasmonic mode of a spherical particle is very specific in the visible light range, and this value is far from the red and near-infrared (NIR) ranges preferred for applications using the solar spectrum or requiring a biological optical transparency window. However, nonspherical plasmonic NPs have a maximum absorption wavelength that can be tuned to the red and NIR photonic regions. Moreover, silver induces a higher intensity than gold,[18] which leads to a stronger plasmon.

Like any resonant mode, when excited by incident electromagnetic waves, LSPR NPs display distinct resonant peaks in both the scattering and absorption spectra. The location of the resonant peaks shifts as a function of several parameters, one among them being the dielectric function of the surrounding medium. Hence, by measuring the shift in the resonant peak in the absorption, for instance, the dielectric function of the surrounding solvent, or of a coating, may be determined.[19]

The simplest LSPR model describes small spheres dispersed in a medium, typically air or water. The interaction with an incident plane wave of a particular frequency is expressed by an analytical expression for the proportion of incident energy absorbed (normalized cross-section). This resonance occurs when the term $\epsilon(\lambda) + 2\epsilon_M$ tends to zero, where $\epsilon(\lambda)$ is the

Received: March 18, 2024
Revised: May 6, 2024
Accepted: June 12, 2024
Published: August 5, 2024

dielectric function of the metal and ϵ_M is the dielectric function of the surrounding medium. When this term vanishes or is minimal, the absorption spectrum displays a peak.

In addition to the existence of a resonant peak, the expression in the denominator also predicts the following: the precise location of the peak will vary depending on the dielectric function of the surrounding medium, ϵ_M. Conversely, by measuring the shift of the resonant peak, λ_*, relative to its location (when the nanoparticle is suspended) in air, the dielectric function of the ambient material ϵ_M may be extracted from the known dispersion of the material $\epsilon(\lambda)$

$$\epsilon_M = -\frac{1}{2}\mathrm{Re}(\epsilon(\lambda_*)) \quad (1)$$

From these equations, it can be concluded that the optical range window of the plasmon can be improved and brought closer to the IR region by changing the dielectric constant of the plasmon environment (as the refractive index of the environment increases, a red shift of the LSPR band can be noticed),[20,21] or alternatively, by changing the size and shape of the particles.[6,18,22−26] Changing the dielectric constant of the environment can be done by replacing the solvent or coating the core with a different dielectric constant shell.[27−29] Coating silver NPs with a different dielectric shell, such as silica, causes a greater red shift than gold NPs.[30] Another advantage of coating NPs with a material inducing a dielectric constant shell is that the layer protects the NPs, prevents them from accumulating together, and provides them with stability.[27,31]

Among the variety of shaped silver NPs, silver nanocubes (NCs) have received particular interest due to their special morphology.[32−41] The sharp corners of silver NCs give additional plasmonic modes and increase the spectrum range.[9] The sharp peaks in the visible−NIR spectrum correspond to the electric dipole (ED), magnetic dipole (MD), electric quadrupole (EQ), magnetic quadrupole (MQ), electric octupole (EO), and magnetic octupole (MO) responses.[9,19,42]

In this study, we propose adding a high-valence cation, namely, Pt(IV), to the dielectric environment of the plasmonic NPs to observe a red shift of the LSPR by increasing the local dielectric constant around Ag NCs and nanowires (NWs). The changes in the refractive index of the surrounding medium as a result of molecules binding to the surface of the metal NPs or the coating can be used as a refractive index sensor.[43] For this, plasmonic metal core dielectric shells were synthesized. Silver NC (and NW) cores were coated with the polydopamine (PDA) nanometric shell using a technique developed in our laboratory,[44] and we adapted it to differently sized silver NCs with different thickness coatings. PDA is a final oxidation product of dopamine-HCl or other catecholamines.[45] That material is widely adopted in science and the chemical industry due to its simplicity, low cost, and adaptability to a variety of scientific and applicative components. PDA has a unique ability to create a uniform and conformal thin layer by a simple coating process.[45−47] The PDA coating can prevent leaching in the aqueous environment.[44] In addition, a thin layer of PDA on Ag NCs improves the sensing of biological molecules through $\pi-\pi$ interactions and hydrogen bonds.[14] In our research, the PDA coating was doped with hexachloroplatinate(IV) complexes at varying concentrations. The Pt(IV) cation was chosen for its high charge and the stability of the cations resulting from their large atomic radii. The absorption spectrum of plasmonic NPs that determines the influence of a cation near the plasmonic particles was measured by ultraviolet−visible (UV−vis) spectroscopy. Rakic's model provides the wavelength dependence of the dielectric function of silver.[48]

2. EXPERIMENTAL SECTION

2.1. Synthesis of Ag NCs. Five milliliters of ethylene glycol (EG) (Aldrich) in a glass vial (27 mL) was heated at 150 °C for 1 h in a silicone oil bath (Pyrex crystallizing dish (115DX65H mm) with 100 mL of silicone oil); the silicone oil level matches the EG level inside the vial. A magnetic stirrer was inserted into the vial and stirred at 250 rpm. One mL of 3 mM HCl in EG was quickly injected into the vial. After 10 min, 3 mL of a 94 mM silver nitrate (STREM, 99.9%) solution in EG and 3 mL of 147 mM poly(vinylpyrrolidone) (PVP) (Aldrich, $M_W \approx 55{,}000$) in EG were injected into the vial using a two-channel syringe pump (Sono-Tek 12−05126) at a rate of 0.75 mL/min. The reaction was done with a stopper, and the magnetic stirrer was on during the entire reaction. The reaction lasted 4 h for 85−100 nm NCs, 6 h for 200−210 nm NCs, and 20 h for NWs. The reaction was ended by removing the vial from the oil bath and letting it cool with magnetic stirring (250 rpm) at room temperature for an hour. The nanomaterials were separated by centrifugation (HERMLE, Z 326 K) at 12,000 rpm for 20 min and redispersed in 20 mL of acetone. The centrifugation was then repeated twice, and the precipitate was redispersed each time in 30 mL of deionized water (DW). Then, the precipitate was redispersed in 10 mL of ethanol.

2.2. Synthesis of the Ag NCs@PDA[$PtCl_6$]$^{2-}$ Core@Shell. For the 10 nm shell on 200 nm NCs, 1 mL of 36 mM dopamine-HCl (Sigma-Aldrich, 99%) was dissolved in DW and 256 μM hexachloroplatinate (IV) (Colonial Metals, Inc.) was added to it. 290 μL of this solution was added to a vial containing 9 mL of Trizma-base buffer solution (pH = 7.5, 0.01 mmol/mL Trizma base 99.9%, Sigma-Aldrich) and 1 mL of silver NC solution. The polymerization process lasted 20 min, under magnetic stirring at R.T. The NCs were washed 4 times with ethanol in a centrifuge at 12,000 rpm for 1 h. Finally, the coated NCs were redispersed in 5 mL of ethanol.

For the 5 nm shell on 145 nm nanorods, 1 mL of 1.5 mM dopamine-HCl was dissolved in DW and 44 μM hexachloroplatinate(IV) was added. 50 μL of this solution was added to a vial containing 9 mL of Trizma-base buffer solution and 1 mL of silver NW solution. All other steps are the same as those on NCs.

2.3. Structural Characterization. The size and shape of the NPs were investigated using an environmental scanning electron microscope (E-SEM) (Quanta FEG 250, FEI) with high vacuum. The structure of the NPs and the thickness of the PDA layer were investigated by using a transmission electron microscopy (TEM) (JEM-1400, JEOL) at 120 kV. In order to investigate the morphology of the layer, high-resolution transmission electron microscopy (HR-TEM) images were acquired on a JEOL-2100 transmission electron microscope operated at 200 kV. Particle size measurement was done by Image-J software.

Qualitative analysis of the PDA layer was investigated by X-ray photoelectron spectroscopy (XPS, Thermo-Scientific, Nexsa) with an Al Kα X-ray source at room temperature, under high vacuum. The spot size of the XPS device is 400 μm, and the etching raster is 1 mm.

https://doi.org/10.1021/acsomega.4c02150
ACS Omega 2024, 9, 35526−35536

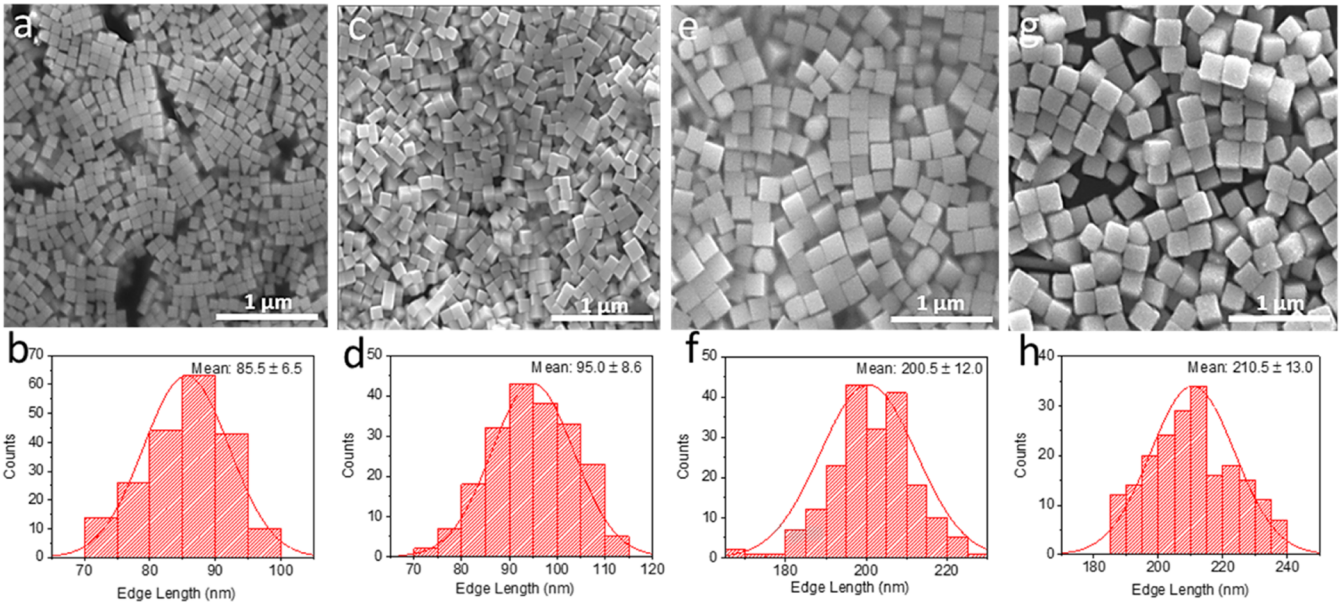

Figure 1. E-SEM images and particle size distribution plot of (a, b) 85 nm, (c, d) 95 nm, (e, f) 200 nm, and (g, h) 210 nm NCs.

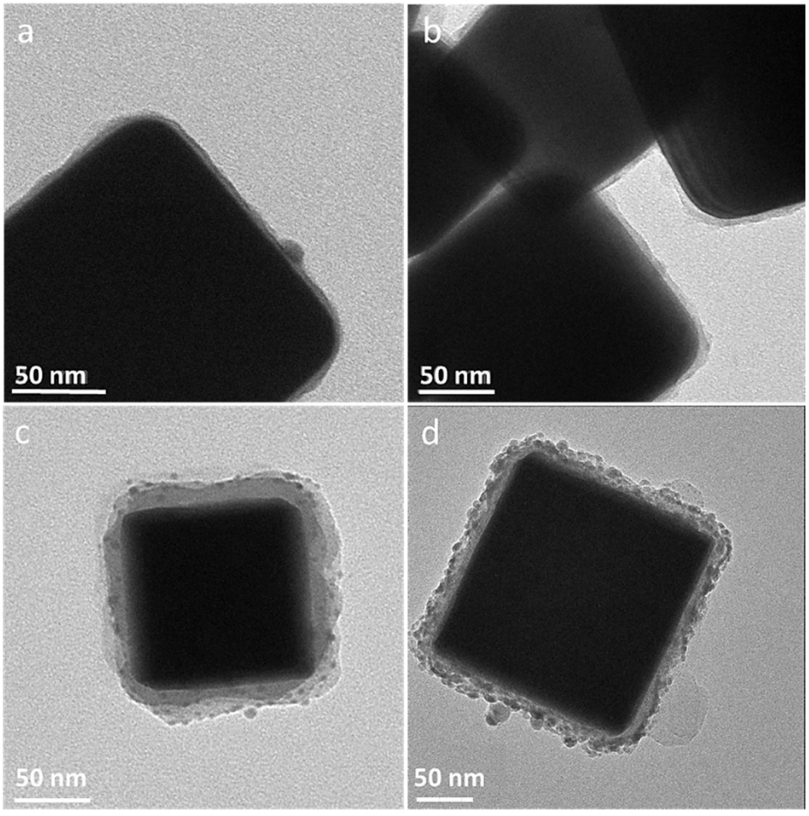

Figure 2. TEM micrographs of (a, b) 200 nm Ag NCs with a 6 nm PDA layer thickness. (c) 95 nm Ag NCs with a 20 nm PDA-Pt layer thickness and (d) 200 nm Ag NCs with an 8 nm PDA-Pt layer thickness.

Quantitative analysis of the PDA layer was investigated by inductively coupled plasma optical emission spectrometry (ICP-OES, Multi view FHX22 SPECTRO ARCOS).

2.4. Spectroscopic Measurements. The spectroscopic measurements of NPs and their comparison with the spectrum of the NPs coated with PDA and the Pt(IV) complex were made using a Varian Cary 5000 UV−vis device.

Based on these measurements, we developed an analytical model to predict the dielectric constant of the coating with MATLAB and Python software.

3. RESULTS AND DISCUSSION

3.1. Synthesis of Ag NCs (and Ag NWs). Ag NCs were synthesized using a published method[35,36] with a few modifications and changes as described in the experimental

https://doi.org/10.1021/acsomega.4c02150
ACS Omega 2024, 9, 35526−35536

section. The synthesis was modified by increasing the temperature by 10 °C, which effectively shortened the process to 5 h, a significant shortening from 15 h or more. Also, limiting the magnetic stirrer rate to 150−300 rpm was necessary since a more vigorous stirring prevents an effective crystallization. With this method, the size of the Ag NCs was controlled from 80 to 200 nm for a 4 to 6 h synthesis, and Ag NWs were formed in syntheses that lasted 20 h or more.

These Ag NCs were synthesized in a typical polyol synthesis[49] as described in eqs 2 and 3

$$2Ag^{+} + 2CH_3CHO \rightarrow CH_3CHO{-}OHCCH_3 + 2Ag + 2H^{+} \quad (2)$$

$$4HNO_3 + 3Ag \rightarrow 3AgNO_3 + NO + 2H_2O \quad (3)$$

In this synthesis, Ag(I) was reduced by ethylene glycol (EG) that was heated to high temperatures (above 140 °C) and used as a solvent eq 2. At these high temperatures, EG reacts to yield acetaldehyde and water. Acetaldehyde reduces Ag cations to metallic Ag and NCs are formed. However, a side reaction occurs where nitric acid reoxidizes Ag(0) eq 3. To prevent that, hydrochloric acid was added to form AgCl and prevent the formation of Ag nitrate. The reaction temperature must be controlled between 130−150 °C to dissolve $AgNO_3$, and finally, to obtain stable nuclei for single crystalline seeds by a redox reaction with EG. Lastly, to generate the geometrical shape of a cube, PVP was introduced dropwise in order to prevent the growth of the {100} faces. Unique colors were characterized in the reaction that changed according to the progress in the various stages of the reaction (Figure S1).

3.2. Size Control of Uncoated NCs. The NC size and morphology of NCs were characterized by scanning electron microscopy (SEM) (Figures 1 and S2−S3). A uniform shape and homogeneous size distribution (∼7% standard deviation) were achieved in each of the samples. The edge-length mean size is distributed around the mean values of 85, 90, 200, and 210 nm as shown by the particle size distribution obtained from particle counting (Figures 1 and S2a). The NWs show a homogeneous diameter with a mean size of 200 nm (Figure S3).

3.3. Conformal NC Coating of PDA and PDA-Pt(IV). The polymerization process of PDA on Ag relies on the room-temperature in situ polymerization of dopamine in a Trizma buffer solution.[14,44] Transmission electron microscopy (TEM) shows the formation of a conformal coating with a thickness varying between 6 and 20 nm (Figures 2 and S4). This protocol has been applied to Ag NCs and NWs (Figure S5). The reaction occurs preferentially on the metallic surface, and no free PDA particles were observed. PDA-coated Ag was used as a control sample in the spectroscopic study.

The pristine Ag NCs were coated with a polymeric layer of polydopamine (PDA) containing Pt(IV) cations (Figures 3 and S6). The in situ polymerization was carried out as previously described, with the addition of hexachloroplatinate-(IV) [$PtCl_6^{2-}$] dissolved in deionized water and added to the Trizma-base buffer solution. The addition of the complex caused the deprotonation of alcohols and initiated the polymerization process[46,47,50] (Figure 4).

The $PtCl_6^{2-}$ complex was added before the PDA polymerization process to ensure the uniform complexation of Pt(IV) by the monomers and the different units of the polymer. The polymerization of dopamine yields multiple amine and imine

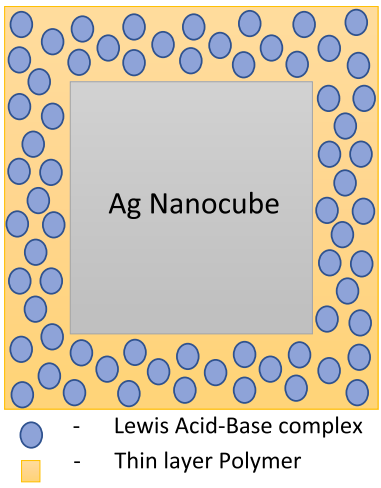

Figure 3. Lewis acid−base complex illustration.

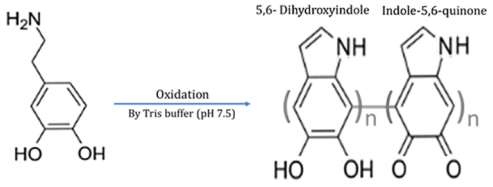

Figure 4. Structure of dopamine before and after polymerization..

groups, which act as ligands for Pt(IV) and replace the soft chloride ligand. A low concentration of the Pt(IV) complex (256 μM) and a short polymerization time (20 min) were used to prevent the galvanic replacement between the Pt(IV) cation and Ag(0) NCs. The polymerization time was determined from a controlled side experiment. The completion of the reaction led to a light brown colored solution (Figure S6), the change of color being attributed to the formation of PDA. The PDA polymerization process was adapted to the coating of Ag NCs, considering their size, after being initially developed for coating plain surfaces of Ag. Contrary to the one-step reaction described above, a two-step reaction, PDA coating followed by the addition of $PtCl_6^{2-}$, resulted in the galvanic displacement of Ag(0) by Pt(IV) (Figure S7).

3.4. X-ray Photoelectron Spectroscopy Characterization of Coated NCs. The Ag@PDA- and Ag@PDA/Pt-coated particles were characterized by TEM and XPS (Figures 2 and 5, respectively). Figure 2a,b shows the 200 nm Ag@PDA NCs. The coating appears relatively homogeneous, conformal, and uniform with a thickness of 6 nm. The coating follows the particle shape and few defects are visible along its length. Figure 2c,b shows 95 and 200 nm Ag@PDA/Pt NCs, respectively. Figure 2d shows a rough polymer coating, but it is relatively uniform with a thickness of 8 nm. Also, Figure 2c shows a coating with a 20 nm thickness since a larger amount of dopamine and Pt(IV) complexes were added to it. Additional TEM images of the coating with different thicknesses are available in the Supporting Information (Figure S8).

The dependence of the PDA layer thickness on the concentration of Pt(IV) was measured by ICP (presented in detail in Section 3.6) and is shown in Figure 6c, which revealed a linear correlation with a slope of 2.85 nm per weight percent of Pt(IV). This suggests that Pt(IV) acts as a catalytic center that increases the polymerization, and therefore, the presence

https://doi.org/10.1021/acsomega.4c02150
ACS Omega 2024, 9, 35526−35536

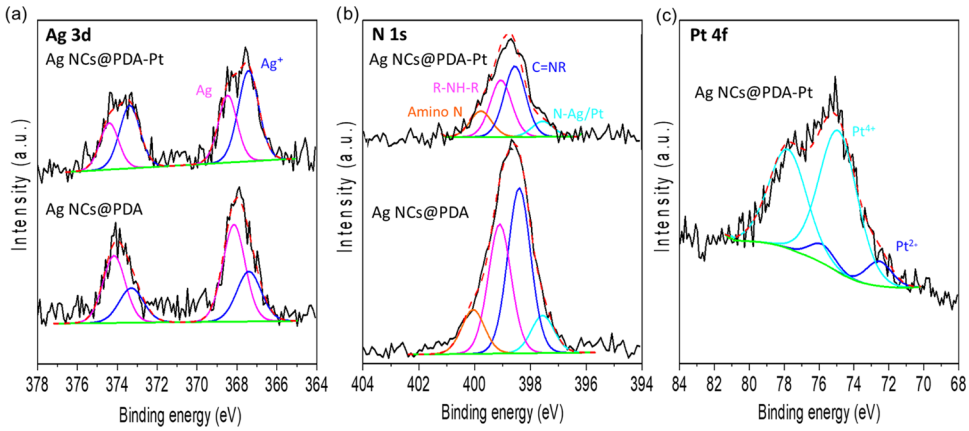

Figure 5. XPS images of Ag NCs coated with PDA-Pt (top) and PDA (down). XPS shows qualitative analysis of (a) Ag 3d, (b) N 1s, and (c) Pt 4f levels.

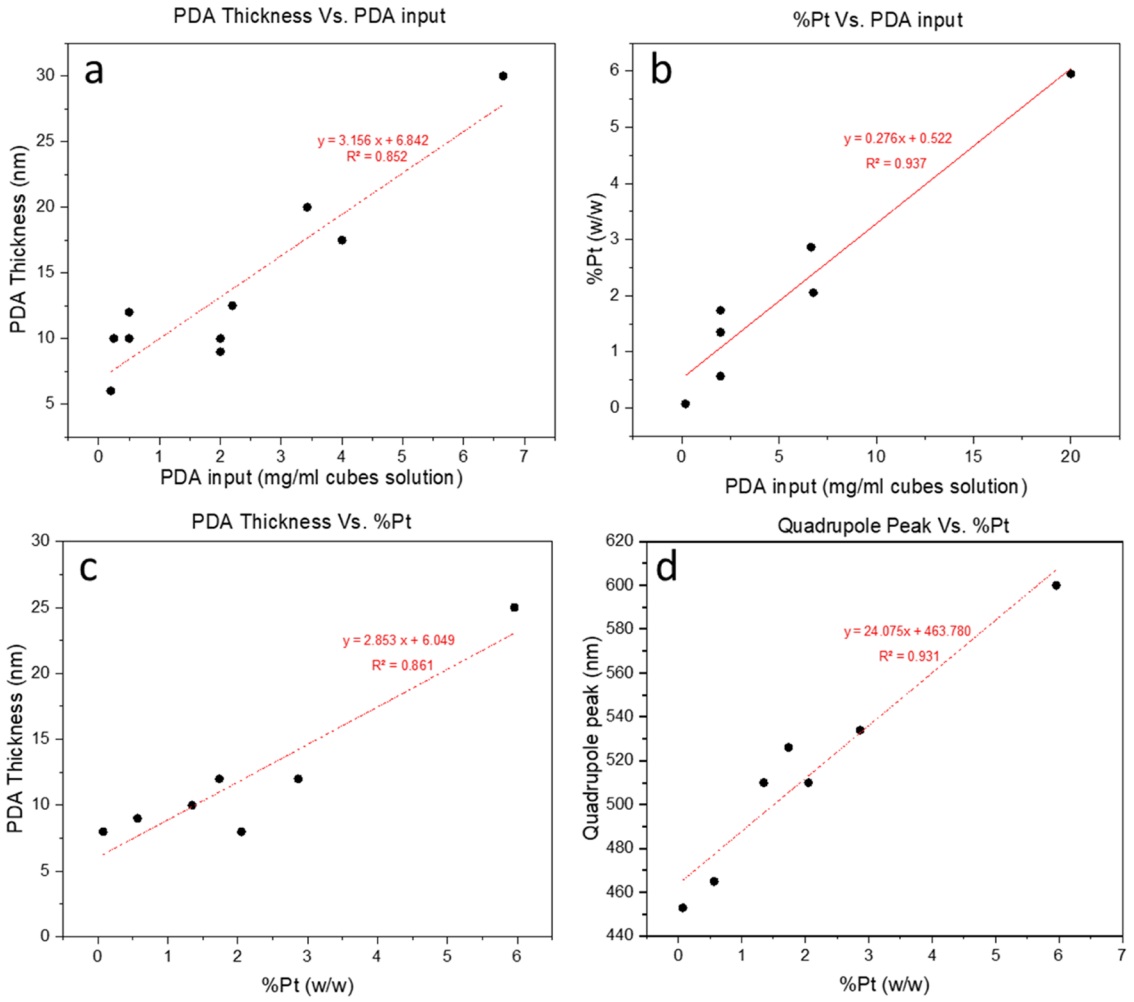

Figure 6. PDA and Pt concentration graphs showing their influence on shell growth and the plasmon resonance shift. (a) PDA thickness (nm) vs PDA input (mg/mL cube solution), (b) %Pt (w/w) vs PDA input (mg/mL cube solution), (c) PDA thickness (nm) vs %Pt (w/w), and (d) quadrupole peak (nm) vs %Pt (w/w).

of roughness was observed only in samples with Pt(IV) complexes. However, to confirm the identity of the Pt(IV) complexes in the polymer layer, we relied on XPS (Figure 5 and Table 1), which rejected the hypothesis of metallic Pt(0) particle formation in the PDA layer. This figure shows XPS results of 200 nm Ag NCs with two types of PDA coatings, with and without Pt(IV) complexes. From the XPS results, we confirmed the absence of metallic Pt(0) in the samples where we added Pt(IV) complexes. On the other hand, in these samples, there is also a relatively higher presence of metallic Ag (3.00%) and Ag(I) (4.46%) than in samples where Pt(IV) complexes were not added (2.36 and 1.57%, respectively). It

https://doi.org/10.1021/acsomega.4c02150
ACS Omega 2024, 9, 35526−35536

Table 1. Quantitative Analysis (w/w) of Silver (Metallic and Cationic), Nitrogen, and Platinum (Metallic and Cationic) Elements According to XPS Results

	Ag^{+}	Ag^{0}	N	Pt^{4+}	Pt^{2+}	Pt^{0}
Ag NCs@PDA	4.46	3.00	85.71	6.10	0.72	0
Ag NCs@PDA/Pt(IV)	1.57	2.63	95.80	0	0	0

appears that even if a galvanic replacement process has occurred, it occurs gently. The reduction of Pt(IV) only causes Pt to decrease from the Pt(IV) (6.1%) to the Pt(II) (0.72%) oxidation states but not beyond that. This is one of the reasons we started from Pt complexes with the maximum oxidation state possible. As for the nitrogen groups, there is no difference between the two samples, as evidenced by peaks that appear at the same energy but in different percentages (95.8 vs 85.71% due to the addition of Pt cations), which confirm the presence of the polymeric coating around the particle and provide a means for a coordinative bond, although it is uncertain whether PDA binds exclusively through the nitrogen atoms, as they may also bind through the double bonds in the aromatic rings of the functional groups or, alternatively, dissolve within the layer in physical bonds. Additionally, we used the XPS results to calculate the percentage of Pt cations and metals from the PDA layer. According to the XPS result, the ratio between the amount of total Pt (cationic and metallic) to the amount of nitrogen is 7:86, respectively. The average ratio that appears in the literature[50] between the number of nitrogen atoms and the number of carbon atoms in the PDA layer is 9:84, respectively. From the calculation of the ratio between them and assuming that our layer includes only carbon atoms, nitrogen, and Pt, it can be evaluated that the amount of Pt in the polymer layer is close to 1% (and the amount of carbon and nitrogen atoms are 89.5 and 9.5%, respectively).

The XPS etching method was performed to obtain information about the PDA-Pt(IV) composition in a layer depth using an ionized Ar gas beam to etch layers of the surface and reveal subsurface information (Figure 7a).

PDA was coated on a 250 nm metallic gold surface to simulate the layers covering the particles and investigate the coating layer; the same synthetic parameters were used to polymerize dopamine. The investigation on the flat surface allows us to use the sputtering mode of the XPS to establish a precise atomic profile of the coating. Such a sputtering technique cannot be applied to nanoparticles.

In Figure 7b, we observed the nitrogen XPS signal decreasing with the removal of surface layers by sputtering, and simultaneously, the XPS signal of gold atoms increases. The sputtering can etch PDA and expose the Au surface to the vacuum chamber of the XPS. We assumed that Pt ions are coordinated by nitrogen in amine, pyridine, or imidazole rings. Indeed, Figure 7c indicates that as the layers are removed, the amount of Pt in the layer decreases. However, even if this phenomenon qualitatively corroborates the coordination model of Pt ions, the decrease is not as significant as for nitrogen atoms. Indeed, the coordinative bond is certainly broken during the sputtering when the sample is bombarded with plasma or high-energy particles. While the plasma evaporates the organic part, Pt remains inside the layer due to its heavier nature.

3.5. UV−Vis Measurements of Coated NCs with the PDA-Pt(IV) Shell. Figures 8 and S2b show a UV−vis spectrum of coated and uncoated 85, 95, and 200 nm Ag NCs. All of the black lines are the basic spectrum of NCs

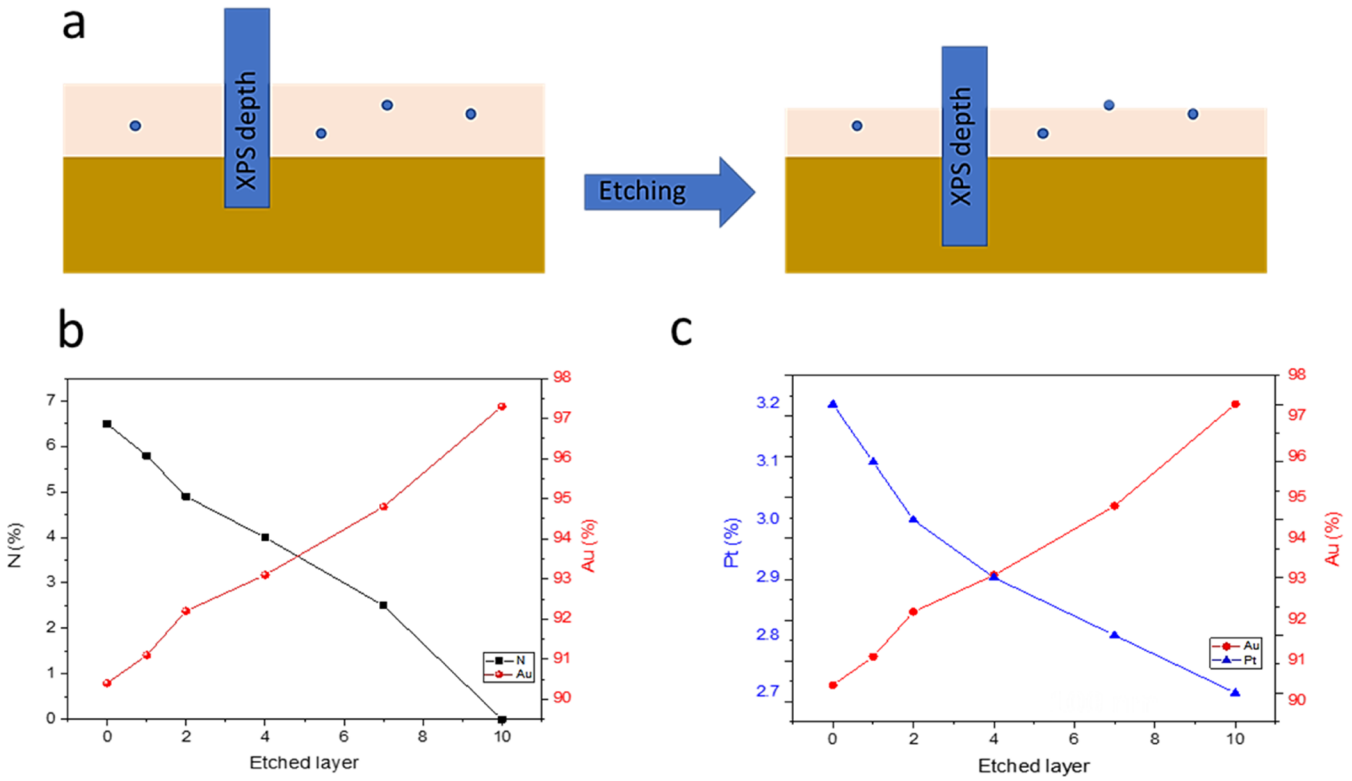

Figure 7. XPS etching method results. (a) Illustration of the XPS etching method. (b) N% and Au% against a number of etched layers. (c) Pt% and Au% against a number of etched layers. All percentages are in w/w.

https://doi.org/10.1021/acsomega.4c02150
ACS Omega 2024, 9, 35526−35536

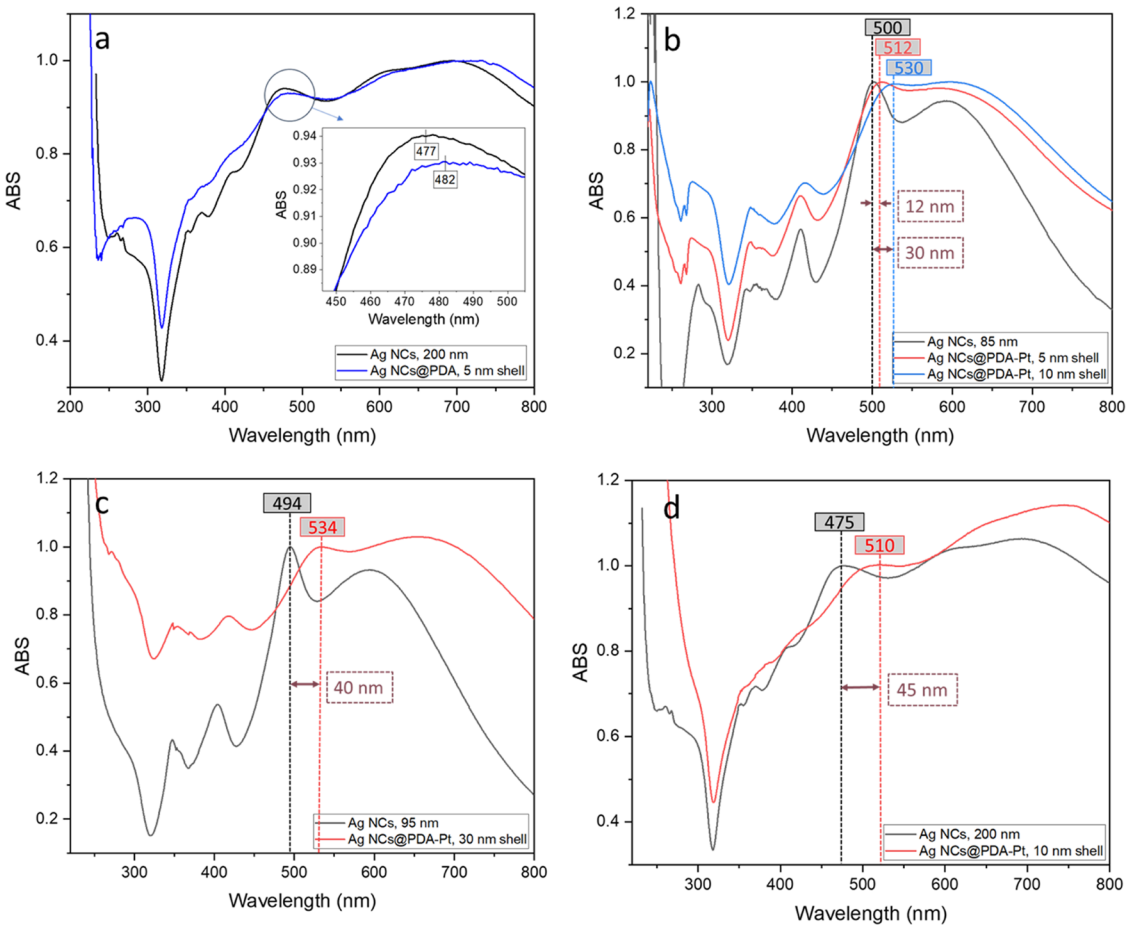

Figure 8. UV−vis spectra of coated and uncoated Ag NCs. (a) Spectrum of 200 nm uncoated and PDA-coated Ag NCs, without Pt. UV−vis spectra of (b) 85 nm, (c) 95 nm, and (d) 200 nm uncoated and PDA-Pt-coated Ag NCs.

without a polymer layer or Pt(IV) complex addition. This figure shows a sharp plasmon resonance for small uncoated NCs (85 and 95 nm, a black line in Figure 8b,c, respectively), whereas 200 nm particles exhibited a spread and broad spectrum (a black line in Figure 8d). Additionally, the spectrum is typical of the particle's cubic shape.

The effect of the coating on the NCs was analyzed by focusing on the quadrupole peak, which is the sharpest with the highest intensity. To obtain an indication of the Pt cation effect on the plasmon resonance frequency, the shift of the coated particle's quadrupole peak and the uncoated particle's quadrupole peak was measured.

The change in the spectrum of 200 nm NCs with a 5 nm PDA coating without Pt(IV) complexes is shown in Figure 8a. The dipole peak was slightly broadened due to an increase in the size of the coated particle. The resulting shift was minimal (about 5 nm). This result is used as a controlled experiment for the research and demonstrates that the nanoparticle spectrum is not significantly affected by a thin coating of PDA.

On the contrary, all of the samples coated with a Pt-rich coating show a significant red shift of the plasmonic resonance. Figure 8b shows an 85 nm NC spectrum with a quadrupole peak at 500 nm and the spectrum of two different thicknesses of thre polymer layer, 5 and 10 nm, with Pt(IV) complex addition. The coated NCs show a shift of 12 and 30 nm, respectively, of the quadrupole. As the polymer layer is thicker, the quadrupole shift increases and the spectrum (mainly in the dipole region) becomes wider as a result of the increase in the particle size. Another effect to be considered is the increased polydispersity of the Ag NCs arising from the cumulative effect of the polydispersity of the Ag core and the polymeric shell. In Figure 8c,d, a higher delta shift of 40 and 45 nm, respectively, is observed for larger particles with a PDA-Pt(IV) layer. Based on these graphs, we can clearly assess the significant effect of the Pt(IV) complexes on the plasmonic resonance, mainly the quadrupole contribution to the spectrum.

Pt(IV) complexed on the surface of Ag plasmonic NCs shifted the resonance to red as a result of the change in the dielectric function at the interface with the Ag metal core. This approach confirms the influence of the cation's complexation in the vicinity of the LSP and opens the way to the investigation of different transition metals complexed on the surface of plasmonic nanoparticles. This approach is particularly significant in the context of promising applications of the LSPR, namely, catalysis with transition metals enhanced by light and sensing of toxic metals.

3.6. Correlation between the Plasmon Resonance Shift and the Pt(IV) Coating. To get the exact amounts of PDA and Pt complexes, we repeated the experiment a statistical number of times and performed a quantitative analysis by chemical analysis (ICP-AES technique). To prepare the samples for analysis, we dried the particles and weighed them. The initial amount of dopamine added to the solution was used to calculate the dependence between the amount of Pt atoms in the polymer layer and the amount of PDA using the ICP results shown in Figure 6b. The amount of Pt atoms

https://doi.org/10.1021/acsomega.4c02150
ACS Omega 2024, 9, 35526−35536

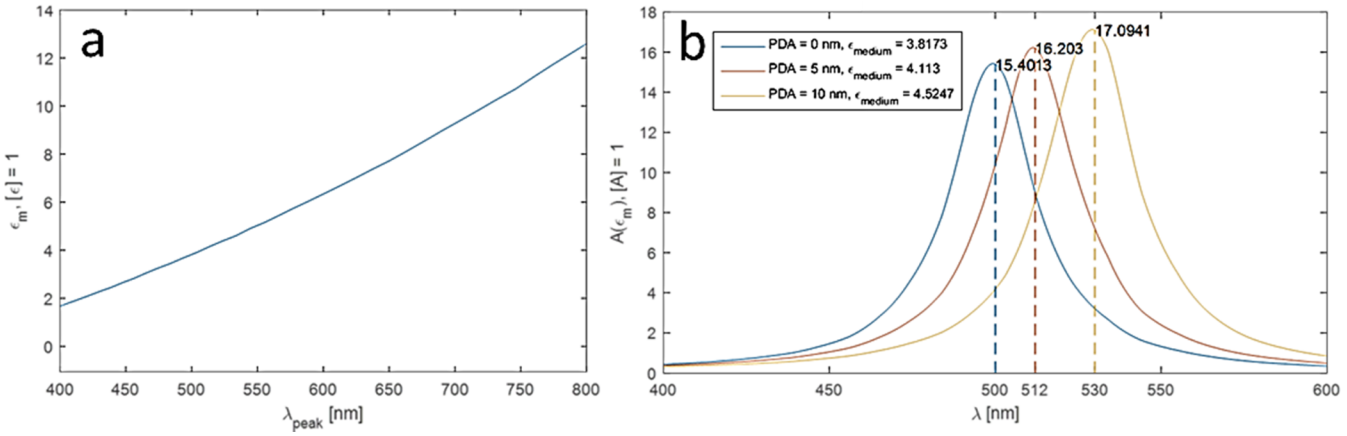

Figure 9. (a) Dielectric constant calibration graph in a medium of 85 nm Ag NCs with a spherical shape and a dipole wavelength between 400 and 800 nm. (b) Absorption curves for different thicknesses of PDA-coated nanospheres; the values for ϵ_M are taken from the calibration graph.

shown in the graphs was calculated as the weight ratio between Pt and Ag, considering the amount of Pt per particle size.

The dependence between the thickness of the PDA layer and the amount of dopamine added to the solution is plotted in Figure 6a, showing a linear relationship with a slope of 3.16 nm coating per mg of dopamine (correlation factor, $R^2 = 0.85$). Figure 6b displays the linear dependence between the initial amount of dopamine and the amount of Pt complexes absorbed in the layer with a slope of 0.28% w/w Pt complexes for every mg of dopamine ($R^2 = 0.94$). Therefore, the amount of dopamine added to the solution can effectively control the coating size and the amount of Pt(IV) complexed in the PDA layer. The dependence between the wavelength of the quadrupole peak and the percentage of Pt complexes in the layer is shown in Figure 6d. We observe a linear correlation ($R^2 = 0.93$) with a slope of 24 nm/wt % Pt(IV) complexes and a constant of 463 nm. In other words, with every 1 wt % Pt absorbed in the coating (the weight ratio between Pt and Ag), the wavelength increases by 24 nm. Similarly, the dependence of the delta shift length on the percentage of Pt absorbed in the layer is shown in Figure S7.

3.7. MATLAB Model of the Dielectric Medium. Localized surface particles (LSPs) display a distinct resonant peak in both the scattering and absorption spectra. The most basic model for such excitations describes small metallic spheres dispersed in a medium, typically air or water. The behavior of the nanostructures can be best predicted and controlled for sizes in which the electrostatic approximation (ESA) is valid: $d \lesssim \lambda/20$, where d is a characteristic length scale such as the diameter of the particle. For radiation in the visible range, with a nominal wavelength of $\lambda \cong 550$ nm, the diameter should thus ideally be smaller than 25 nm.

When radiation, modeled as a plane wave, is incident on one such metallic nanosphere, the normalized absorption cross-section can be expressed as

$$\sigma_n \equiv \frac{\sigma}{\pi a^2} = 4\sqrt{\epsilon_M}\frac{2\pi}{\lambda}\frac{3\epsilon_M \mathrm{Im}\epsilon(\lambda)}{|\epsilon(\lambda) + 2\epsilon_M|^2}E_0 \quad (4)$$

where $\epsilon(\lambda)$ is the dielectric function of the metal, e.g., Ag, composing the sphere, and ϵ_M is the dielectric function in the surrounding medium. (It should be noted that λ denotes the wavelength in vacuum rather than in the medium). The normalized absorption cross-section is defined as the ratio of the cross-section to the geometric cross-section and can be shown to express the proportion of incident energy, which is absorbed by the nanoparticle.

The existence of a resonant peak can be understood using the expression above: due to dispersion, the dielectric function of the nanostructure material is frequency-dependent, $\epsilon = \epsilon(\lambda)$; for a plasmonic material, the (real part of) dielectric function is negative. At the peak wavelength, the denominator vanishes, and the expression diverges. More precisely, the denominator is an expression in complex variables: in Ag, the dielectric function has a nonzero imaginary part due to absorption. For a transparent medium with minimal absorption, the imaginary part of the dielectric function of the medium may be neglected, but for an absorbing medium such as PDA, this is not the case. Nonetheless if the imaginary parts of the dielectric function of Ag and of the medium are sufficiently flat over the optical range, then the conclusion is the same: the denominator is minimal and thus the absorption shows a peak at the wavelength, which satisfies (as mentioned in the introduction) the equation

$$\mathrm{Re}(\epsilon(\lambda)) + 2\epsilon_M = 0 \quad (5)$$

In principle, the dielectric function of the medium may also display dispersion, so that the relation above holds precisely only at the resonance wavelength. In practice, however, the index of refraction of the medium, and hence ϵ_M, is typically quite flat throughout the optical region, much more so than that of the metal, and so this can be used to obtain a value for ϵ_M which is valid for most, if not all, of the optical range.

The foregoing discussion suggests the following method to determine the dielectric function of a medium, such as a coating, in the immediate vicinity of a plasmonic nanostructure. First, the absorption spectrum of the coated nanoparticles (suspended in solution) is measured, e.g., by a spectrophotometer or by UV−vis spectrometry. Next, the resulting spectrum is analyzed, and the peak wavelength is extracted. Third, the peak wavelength is used to retrieve the value of the dielectric function of the metal, $\epsilon(\lambda)$, from known tabulated values, determined either empirically or using an analytic model. Finally, the value determined for $\epsilon(\lambda)$ is inserted into the resonance expression above rendering the value of the dielectric function of the medium, specifically eq 1.

Some comments are in order:

1. The model considers only the effect of the coating, while that of the solvent beyond is neglected. (If no coating is

https://doi.org/10.1021/acsomega.4c02150
ACS Omega 2024, 9, 35526−35536

applied, the solvent, like ethanol, water, etc., is then properly considered the medium.) This assumes that the coating thickness is sufficient so that the plasmon field decays entirely within and the interaction with the solvent is negligible. Otherwise, a model for a stratified system must be used. Order-of-magnitude calculations suggest that a thickness of 10−20 nm is sufficient.

2. The model is accurate for spherical nanoparticles of sizes obeying the limits discussed above. Ag NCs, with characteristic length scales ranging from 80−250 nm, depart significantly from this range of validity, and the simplified model, quite the proverbial "spherical cow", cannot be expected to give better than an order-of-magnitude estimate for the value of the dielectric function.

The method presented can be tested in the case of nanoparticles with no coating, in which case the solvent is the medium. The prediction of the model can be compared with data available independently for the solvent. In the optical range, ethanol is transparent, and the dielectric function is known to assume the real value $\epsilon_M = 1.83$ flat across the optical range.[51,52]

To this end, the absorption spectrum of the Ag NCs suspended in ethanol was measured using a UV−vis spectrometer. A characteristic resonant curve was found with a peak wavelength $\lambda = 500$ nm. This was then referred to the Rakic model for the optical properties of Ag[48] to extract the dielectric function at the resonance of the latter. When substituted into the resonance relation eq 5, this renders a value for the dielectric function ϵ_M of surrounding ethanol. This is demonstrated in Figure 9a, which shows the measured value of $\lambda_{resonance}$, the calibration curve which follows from the resonance relation when the Rakic data[48] is substituted for $\epsilon(\lambda)$, and the predicted value of $\epsilon_M = 3.8$. From the graph, it can be concluded for NCs coated with (pure) PDA: $\lambda = 512$ nm, giving $\epsilon_M = 4.1$, and for the PDA coating doped with Pt(IV) complexes: $\lambda = 530$ nm, giving $\epsilon_M = 4.5$.

Figure 9b exemplifies absorption curves for nanospheres assuming a calculation of the value ϵ_M according to the calculation curve shown in Figure 9a. From the test case of ethanol, however, it is clear that while the order of magnitude is on target, the divergence of the model's predictions from the precisely known value is significant.

4. CONCLUSIONS

In this research work, we succeeded in embedding the Pt(IV) cations in a PDA layer on the surface of Ag LSPR NCs and NWs as a model for a highly dielectric layer on the LSPR particles. The Ag LSPR nanocubes were characterized by SEM, TEM, XPS, and ICP analysis. According to microscopic, spectroscopic, and quantitative analyses, we discovered the catalytic role of Pt(IV) complexes to tune the thickness of the PDA layer; the PDA thickness increases at a ratio of 3 nm/wt % of Pt(IV). As part of the synthetic process, we were able to synthesize Ag nanocubes of different sizes (80 to 200 nm) and conformally coat PDA dielectric layers in different thicknesses from 5 to 20 nm and up to 1 wt % Pt(IV) in the shell. All of the Ag nanocubes display a complex plasmonic resonance from the spectroscopic measurements, and the dielectric PDA coating with the embedded Pt(IV) cations red-shifts the main resonance by up to 45 nm, which linearly correlates with the increase of the dielectric constant of the shell and the thickness of the shell. A numerical model of the dielectric medium enables us to calculate the dielectric constant of the medium of the coated particle (PDA-Pt) and predict the maximum dipole peak of the LSPR NCs. Following this proof-of-the-concept study, we believe that the study can be extended to different plasmonic metals and we propose to investigate the ligand design of the Pt active site within the polydopamine matrix and take advantage of the catalytic nature of Pt complexes toward light-induced catalysis[53] and chemical-sensing experiments.

■ ASSOCIATED CONTENT

Supporting Information

The Supporting Information is available free of charge at https://pubs.acs.org/doi/10.1021/acsomega.4c02150.

Photographs of the experimental setup and the colors of the solutions; additional scanning electron microscopy; transmission electron microscopy, and absorption spectrum of the pristine Ag NCs (PDF)

■ AUTHOR INFORMATION

Corresponding Author

David Zitoun − *Department of Chemistry and Bar Ilan Institute of Nanotechnology and Advanced Materials (BINA), Bar Ilan University, Ramat Gan 5290002, Israel;* orcid.org/0000-0003-3383-6165; Email: david.zitoun@biu.ac.il

Authors

Avi Huri − *Department of Chemistry and Bar Ilan Institute of Nanotechnology and Advanced Materials (BINA), Bar Ilan University, Ramat Gan 5290002, Israel*

Yaakov Mandelbaum − *Department of Chemistry and Bar Ilan Institute of Nanotechnology and Advanced Materials (BINA), Bar Ilan University, Ramat Gan 5290002, Israel; Department of Applied Physics/Electro-Optics Engineering, Advanced Lab for Electro-Optics Simulations (ALEO), Lev Academic Center, Jerusalem 9116001, Israel*

Mike Rozenberg − *Department of Chemistry and Bar Ilan Institute of Nanotechnology and Advanced Materials (BINA), Bar Ilan University, Ramat Gan 5290002, Israel;* orcid.org/0009-0001-2017-9728

Anya Muzikansky − *Department of Chemistry and Bar Ilan Institute of Nanotechnology and Advanced Materials (BINA), Bar Ilan University, Ramat Gan 5290002, Israel*

Melina Zysler − *Department of Chemistry and Bar Ilan Institute of Nanotechnology and Advanced Materials (BINA), Bar Ilan University, Ramat Gan 5290002, Israel*

Complete contact information is available at: https://pubs.acs.org/10.1021/acsomega.4c02150

Notes

The authors declare no competing financial interest.

■ ACKNOWLEDGMENTS

This work was partially funded by the Israel Innovation Authority through a Kamin grant.

■ REFERENCES

(1) Wang, C.; Meloni, M. M.; Wu, X.; Zhuo, M.; He, T.; Wang, J.; Wang, C.; Dong, P. Magnetic Plasmonic Particles for SERS-Based

Bacteria Sensing: A Review. *AIP Adv.* **2019**, *9* (1), No. 010701, DOI: 10.1063/1.5050858.
(2) Noguez, C. Optical Properties of Isolated and Supported Metal Nanoparticles. *Opt. Mater.* **2005**, *27* (7), 1204−1211.
(3) Farooq, S.; de Araujo, R. E. Engineering a Localized Surface Plasmon Resonance Platform for Molecular Biosensing. *Open J. Appl. Sci.* **2018**, *08* (03), 126−139.
(4) Bolaños, K.; Kogan, M. J.; Araya, E. Capping Gold Nanoparticles with Albumin to Improve Their Biomedical Properties. *Int. J. Nanomed.* **2019**, *14*, 6387−6406.
(5) Jain, P. K.; Huang, X.; El-Sayed, I. H.; El-Sayed, M. A. Review of Some Interesting Surface Plasmon Resonance-Enhanced Properties of Noble Metal Nanoparticles and Their Applications to Biosystems. *Plasmonics* **2007**, *2* (3), 107−118.
(6) Anker, J. N.; Hall, W. P.; Lyandres, O.; Shah, N. C.; Zhao, J.; Van Duyn, R. P. Biosensing with Plasmonic Nanosensors. *Nat. Mater.* **2008**, *7*, 442−453.
(7) Das, G.; Coluccio, M. L.; Alrasheed, S.; Giugni, A.; Allione, M.; Torre, B.; Perozziello, G.; Candeloro, P.; Di Fabrizio, E. Plasmonic Nanostructures for the Ultrasensitive Detection of Biomolecules. *Riv. Nuovo Cimento* **2016**, *39* (11), 547−586.
(8) Kim, M.; Lee, J.; Nam, J. Plasmonic Photothermal Nanoparticles for Biomedical Applications. *Adv. Sci.* **2019**, *6* (17), No. 1900471.
(9) González, A. L.; Noguez, C. Influence of Morphology on the Optical Properties of Metal Nanoparticles. *J. Comput. Theor. Nanosci.* **2007**, *4* (2), 231−238.
(10) Clavero, C. Plasmon-Induced Hot-Electron Generation at Nanoparticle/Metal-Oxide Interfaces for Photovoltaic and Photocatalytic Devices. *Nat. Photonics* **2014**, *8* (2), 95−103.
(11) Atwater, H. A.; Polman, A. Plasmonics for Improved Photovoltaic Devices. *Nat. Mater.* **2010**, *9* (3), 205−213.
(12) Zhang, X.; Chen, Y. L.; Liu, R.-S.; Tsai, D. P. Plasmonic Photocatalysis. *Rep. Prog. Phys.* **2013**, *76* (4), No. 046401.
(13) Hou, W.; Cronin, S. B. A Review of Surface Plasmon Resonance-Enhanced Photocatalysis. *Adv. Funct Mater.* **2013**, *23* (13), 1612−1619.
(14) Tegegne, W. A.; Mekonnen, M. L.; Beyene, A. B.; Su, W.-N.; Hwang, B.-J. Sensitive and Reliable Detection of Deoxynivalenol Mycotoxin in Pig Feed by Surface Enhanced Raman Spectroscopy on Silver Nanocubes@polydopamine Substrate. *Spectrochim. Acta, Part A* **2020**, *229*, No. 117940.
(15) Liu, J.; He, H.; Xiao, D.; Yin, S.; Ji, W.; Jiang, S.; Luo, D.; Wang, B.; Liu, Y. Recent Advances of Plasmonic Nanoparticles and Their Applications. *Materials* **2018**, *11* (10), No. 1833.
(16) Martinsson, E.; Otte, M. A.; Shahjamali, M. M.; Sepulveda, B.; Aili, D. Substrate Effect on the Refractive Index Sensitivity of Silver Nanoparticles. *J. Phys. Chem. C* **2014**, *118* (42), 24680−24687.
(17) Noguez, C. Surface Plasmons on Metal Nanoparticles: The Influence of Shape and Physical Environment. *J. Phys. Chem. C* **2007**, *111* (10), 3806−3819.
(18) Amendola, V.; Bakr, O. M.; Stellacci, F. A Study of the Surface Plasmon Resonance of Silver Nanoparticles by the Discrete Dipole Approximation Method: Effect of Shape, Size, Structure, and Assembly. *Plasmonics* **2010**, *5* (1), 85−97.
(19) Mahmoud, M. A.; Chamanzar, M.; Adibi, A.; El-Sayed, M. A. Effect of the Dielectric Constant of the Surrounding Medium and the Substrate on the Surface Plasmon Resonance Spectrum and Sensitivity Factors of Highly Symmetric Systems: Silver Nanocubes. *J. Am. Chem. Soc.* **2012**, *134* (14), 6434−6442.
(20) Chen, H.; Kou, X.; Yang, Z.; Ni, W.; Wang, J. Shape- and Size-Dependent Refractive Index Sensitivity of Gold Nanoparticles. *Langmuir* **2008**, *24* (10), 5233−5237.
(21) Garcia, M. A.; García, M. A. Surface Plasmons in Metallic Nanoparticles: Fundamentals and Applications Surface Plasmons in Metallic Nanoparticles Surface Plasmons in Metallic Nanoparticles: Fundamentals and Applications. *J. Phys. D: Appl. Phys.* **2011**, *44* (28), No. 283001.
(22) Yue, Z.; Cai, B.; Wang, L.; Wang, X.; Gu, M. Intrinsically Core-Shell Plasmonic Dielectric Nanostructures with Ultrahigh Refractive Index. *Sci. Adv.* **2016**, *2* (3), No. e1501536, DOI: 10.1126/sciadv.1501536.
(23) Sepúlveda, B.; Angelomé, P. C.; Lechuga, L. M.; Liz-Marzán, L. M. LSPR-Based Nanobiosensors. *Nano Today* **2009**, *4* (3), 244−251.
(24) Liz-Marzán, L. M. Tailoring Surface Plasmons through the Morphology and Assembly of Metal Nanoparticles. *Langmuir* **2006**, *22* (1), 32−41.
(25) Jeon, J. W.; Zhou, J.; Geldmeier, J. A.; Ponder, J. F.; Mahmoud, M. A.; El-Sayed, M.; Reynolds, J. R.; Tsukruk, V. V. Dual-Responsive Reversible Plasmonic Behavior of Core-Shell Nanostructures with PH-Sensitive and Electroactive Polymer Shells. *Chem. Mater.* **2016**, *28* (20), 7551−7563.
(26) Jiang, N.; Zhuo, X.; Wang, J. Active Plasmonics: Principles, Structures, and Applications. *Chem. Rev.* **2018**, *118* (6), 3054−3099.
(27) Yu, P.; Yao, Y.; Wu, J.; Niu, X.; Rogach, A. L.; Wang, Z. Effects of Plasmonic Metal Core -Dielectric Shell Nanoparticles on the Broadband Light Absorption Enhancement in Thin Film Solar Cells. *Sci. Rep.* **2017**, *7* (1), No. 7696.
(28) Miller, M. M.; Lazarides, A. A. Sensitivity of Metal Nanoparticle Surface Plasmon Resonance to the Dielectric Environment. *J. Phys. Chem. B* **2005**, *109* (46), 21556−21565.
(29) Jiang, N.; Shao, L.; Wang, J. (Gold Nanorod Core)/(Polyaniline Shell) Plasmonic Switches with Large Plasmon Shifts and Modulation Depths. *Adv. Mater.* **2014**, *26* (20), 3282−3289.
(30) Avşar, D.; Ertürk, H.; Mengüc, M. P. Plasmonic Responses of Metallic/Dielectric Core-Shell Nanoparticles on a Dielectric Substrate. *Mater. Res. Express* **2019**, *6* (6), No. 065006.
(31) Park, H. S.; Kim, J. Y.; Kim, M. W.; Cho, Y. H.; Kwon, M. K. Localized Surface Plasmon-Enhanced Emission from Red Phosphor with Au-SiO2 Nanoparticles. *Mater. Lett.* **2017**, *205*, 145−149.
(32) Pastoriza-Santos, I.; Liz-Marzán, M. Formation and Stabilization of Silver Nanoparticles through Reduction by N,N-Dimethylformamide. *Langmuir* **1999**, *15* (4), 948−951.
(33) Pastoriza-Santos, I.; Liz-Marzán, L. M. Synthesis of Silver Nanoprisms in DMF. *Nano Lett.* **2002**, *2* (8), 903−905.
(34) Yu, R.; Liz-Marzán, L. M.; De Abajo, F. J. G. Universal Analytical Modeling of Plasmonic Nanoparticles. *Chem. Soc. Rev.* **2017**, *46* (22), 6710−6724.
(35) Siekkinen, A. R.; McLellan, J. M.; Chen, J.; Xia, Y. Rapid Synthesis of Small Silver Nanocubes by Mediating Polyol Reduction with a Trace Amount of Sodium Sulfide or Sodium Hydrosulfide. *Chem. Phys. Lett.* **2006**, *432* (4−6), 491−496.
(36) Im, S. H.; Yun, T. L.; Wiley, B.; Xia, Y. Large-Scale Synthesis of Silver Nanocubes: The Role of HCl in Promoting Cube Perfection and Monodispersity. *Angew. Chem., Int. Ed.* **2005**, *44* (14), 2154−2157.
(37) Rycenga, M.; Cobley, C. M.; Zeng, J.; Li, W.; Moran, C. H.; Zhang, Q.; Qin, D.; Xia, Y. Controlling the Synthesis and Assembly of Silver Nanostructures for Plasmonic Applications. *Chem. Rev.* **2011**, *111* (6), 3669−3712.
(38) Wiley, B.; Sun, Y.; Mayers, B.; Xia, Y. Shape-Controlled Synthesis of Metal Nanostructures: The Case of Silver. *Chem. - Eur. J.* **2005**, *11* (2), 454−463.
(39) Gao, B.; Arya, G.; Tao, A. R. Self-Orienting Nanocubes for the Assembly of Plasmonic Nanojunctions. *Nat. Nanotechnol.* **2012**, *7* (7), 433−437.
(40) Tao, A.; Sinsermsuksakul, P.; Yang, P. Polyhedral Silver Nanocrystals with Distinct Scattering Signatures. *Angew. Chem.* **2006**, *118* (28), 4713−4717.
(41) Gurunatha, K. L.; Marvi, S.; Arya, G.; Tao, A. R. Computationally Guided Assembly of Oriented Nanocubes by Modulating Grafted Polymer-Surface Interactions. *Nano Lett.* **2015**, *15* (11), 7377−7382.
(42) Willets, K. A.; Van Duyne, R. P. Localized Surface Plasmon Resonance Spectroscopy and Sensing. *Annu. Rev. Phys. Chem.* **2007**, *58*, 267−297.
(43) Tokarev, I.; Minko, S. Tunable Plasmonic Nanostructures from Noble Metal Nanoparticles and Stimuli-Responsive Polymers. *Soft Matter* **2012**, *8* (22), 5980−5987.

https://doi.org/10.1021/acsomega.4c02150
ACS Omega 2024, 9, 35526−35536

(44) Kitayev, A.; Zysler, M.; Hardisty, S.; Page, M.; Tal-Gutelmacher, E.; Zitoun, D. Silver Oxygen Reduction Electrocatalyst in Alkaline Medium: Aging and Protective Coating. *Energy Technol.* **2021**, *9* (12), No. 2100546, DOI: 10.1002/ente.202100546.
(45) Ball, V. Polydopamine Nanomaterials: Recent Advances in Synthesis Methods and Applications. *Front. Bioeng. Biotechnol.* **2018**, *6*, No. 109, DOI: 10.3389/fbioe.2018.00109.
(46) Liebscher, J. Chemistry of Polydopamine − Scope, Variation, and Limitation. *Eur. J. Org. Chem.* **2019**, *2019* (31−32), 4976−4994.
(47) Ryu, J. H.; Messersmith, P. B.; Lee, H. Polydopamine Surface Chemistry: A Decade of Discovery. *ACS Appl. Mater. Interfaces* **2018**, *10* (9), 7523−7540.
(48) Rakić, A. D.; Djurišić, A. B.; Elazar, J. M.; Majewski, M. L. Optical Properties of Metallic Films for Vertical-Cavity Optoelectronic Devices. *Appl. Opt.* **1998**, *37*, 5271−5283.
(49) Fievet, F.; Lagier, J. P.; Blin, B.; Beaudoin, B.; Figlarz, M. Homogeneous and Heterogeneous Nucleations in the Polyol Process for the Preparation of Micron and Submicron Size Metal Particles. *Solid State Ionics* **1989**, *32*−*33*, 198−205.
(50) Tyo, A.; Welch, S.; Hennenfent, M.; Fooroshani, P. K.; Lee, B. P.; Rajachar, R. Development and Characterization of an Antimicrobial Polydopamine Coating for Conservation of Humpback Whales. *Front. Chem.* **2019**, *7*, No. 618, DOI: 10.3389/fchem.2019.00618.
(51) Rheims, J.; Köser, J.; Wriedt, T. Refractive-Index Measurements in the near-IR Using an Abbe Refractometer. *Meas. Sci. Technol.* **1997**, *8*, 601−605.
(52) Kedenburg, S.; Vieweg, M.; Gissibl, T.; Giessen, H. Linear Refractive Index and Absorption Measurements of Nonlinear Optical Liquids in the Visible and Near-Infrared Spectral Region. *Opt. Mater. Express* **2012**, *2* (11), 1588−1611.
(53) Qi, M. Y.; Tang, Z. R.; Xu, Y. J. Near Field Scattering Optical Model-Based Catalyst Design for Artificial Photoredox Transformation. *ACS Catal.* **2023**, *13* (6), 3971−3982.

https://doi.org/10.1021/acsomega.4c02150
ACS Omega 2024, 9, 35526−35536